PAPER

Check for updates

Photoresponsive amphiphilic block macrocycles bearing azobenzene side chains†

Lishan Li, Ye Cai, Zhengbiao Zhang, Wei Zhang, Nianchen Zhou* and Xiulin Zhu*

Topological molecular architectures play a crucial role in the self-assembly of amphiphilic block copolymers. Many characteristics of macromolecules originate from the special properties of the ends of molecules. Herein, we synthesized well-defined cyclic block copolymers bearing hydrophobic azobenzene and hydrophilic carboxyl moieties in their side-chains, cyclic-PBHME$_m$-*b*-PAA$_n$, via sequential atom transfer radical polymerization (ATRP) and intramolecular Cu(I)-catalyzed azide/alkyne cycloaddition (CuAAC) cyclization reaction followed by the selective hydrolysis of *tert*-butyl ester. The successful synthesis of the amphiphilic block copolymers was fully characterized via conventional gel permeation chromatography, triple detection gel permeation chromatography, nuclear magnetic resonance, Fourier transform infrared spectroscopy, and matrix-assisted laser desorption ionization time-of-flight mass spectrometry. Via investigating the properties of the cyclic polymer, we observed that the cyclic structure displayed faster photoisomerization in solution than its linear precursor. Moreover, the cyclic copolymer exhibits larger changes in the size and morphology of the self-assembled aggregates upon 365 nm light irradiation as compared to its linear counterpart. These interesting findings show that the topological cyclic architecture greatly affects the photoisomerization of azobenzene and copolymeric packing behavior in micellar aggregates.

Introduction

Aggregates with various morphologies can be achieved via the self-assembly of amphiphilic block copolymers in solution.[1–3] These functional polymeric nanoparticles have become progressively important for the development of new materials, such as drug delivery vehicles, and as biological cell models.[4–7] Over the last few decades, the synthesis, self-assembly, and extensive applications of new polymeric amphiphiles have been receiving significant attention.

Responsive polymers, capable of responding to external stimuli such as pH, redox, and light irradiation, exhibit novel and interesting performances owing to reversible or irreversible changes in their physical properties.[8–12] As is known, the reversible transformation between *trans*- and *cis*-azobenzene can be induced via irradiation with UV light and reversed upon heating or irradiation with visible light. The photo-isomerization of azobenzene chromophores can trigger the change in the properties of azobenzene compounds due to the

differences in the shape and dipole moment of *trans*- and *cis*-azobenzene.[13–17] In addition, azobenzene can undergo cleavage of the azo bond upon treatment with some reductives or azor-eductase. Notably, polymeric azobenzene amphiphiles display versatile properties, such as micelle dissociation, colloid deformation, and vesicle bursting and fusion, and promising applications for various nanostructures in the self-assembly systems.[18–28] Polymer-based azobenzene, as one of the most attractive responsive materials, has been subjected to extensive investigation.[13,29–35]

As one of the most important topological polymers, cyclic polymers represent an interesting class of materials since they usually exhibit unique and improved properties as compared to their linear analogues.[36–45] Recent advances in macrocycles have demonstrated that the cyclic architecture displays profound effects on the photo-responsive properties, such as liquid crystal formation, birefringence, fluorescence emission, and photoin-duced surface relief grating formation, of azobenzene-containing polymers.[46–48] Moreover, the self-assembly behavior and properties of amphiphilic copolymers are also found to be sensitive to the endless topology such as morphology, particle dimension, and stability of the self-assembled aggregates.[49–56]

Rational macromolecular design inspired us to construct cyclic polymeric azobenzene amphiphiles to gain new insights into their structure–property relationship. Herein, we designed and synthesized cyclic amphiphilic block copolymers bearing

State and Local Joint Engineering Laboratory for Novel Functional Polymeric Materials, Jiangsu Key Laboratory of Advanced Functional Polymer Design and Application, College of Chemistry, Chemical Engineering and Materials Science, Soochow University, Suzhou, 215123, P. R. China. E-mail: nczhou@suda.edu.cn; xlzhu@suda.edu.cn

† Electronic supplementary information (ESI) available: Materials, polymer characterization data, DLS and UV-vis data. See DOI: 10.1039/c7ra06688k
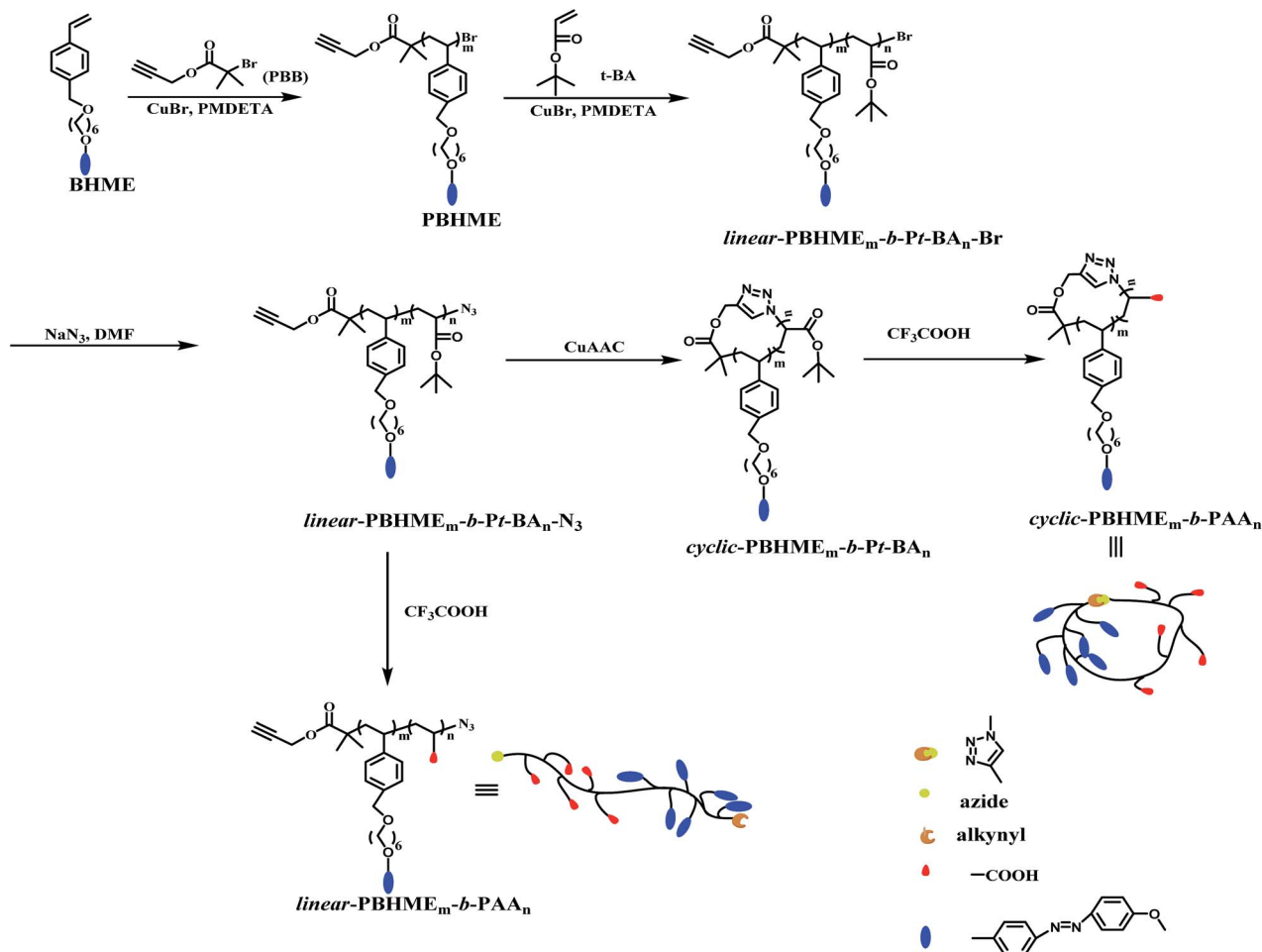
Scheme 1 Synthetic routes for linear-PBHME$_m$-b-PAA$_n$ and cyclic-PBHME$_m$-b-PAA$_n$.

pendent hydrophobic azobenzene and hydrophilic carboxyl groups, cyclic-PBHME$_m$-b-PAA$_n$, *via* successive atom transfer radical copolymerization (ATRP), Cu(ı)-catalyzed azide/alkyne cycloaddition (CuAAC) click chemistry,[57] and selective hydrolysis of *tert*-butyl ester. The synthetic routes for cyclic-PBHME$_m$-b-PAA$_n$ are shown in Scheme 1. Furthermore, we mainly investigated the self-assembly behavior and photoresponsive performance of the resultant cyclic amphiphile; it was observed that the cyclic topology endowed unique properties to cyclic-PBHME$_m$-b-PAA$_n$ as compared to that of its linear counterpart.

Results and discussion

Synthesis and characterization of linear-PBHME$_m$-b-Pt-BA$_n$ and cyclic-PBHME$_m$-b-Pt-BA$_n$

The synthetic routes for linear- and cyclic-PBHME$_m$-b-PAA$_n$ are shown in Scheme 1. The ATRP initiator propargyl-2-bromoisobutyrate (PBB) with an terminal alkyne and styrene monomer bearing azobenzene [[6-(4-benzyloxy)hexyloxy)-(4-methoxyphenyl-azo)]ethylene (BHME) were prepared according to previous study.[58] First, the homopolymer (PBHME) with α-alkyne-ω-bromine was synthesized *via* ATRP polymerization of the functionalized monomer BHME in anisole using the PBB

initiator. The molecular weights of the PBHME were roughly evaluated from the feeding ratio of the reactants and polymerization conversion. PBHME$_{10}$ with 10 repeating BHME units (m) was obtained, based on the ^{1}H NMR spectra of PBHME (Fig. S1†) and calculation according to Formula S1.† The block copolymers with α-alkyne-ω-bromine, linear-PBHME$_m$-b-Pt-BA$_n$-Br, were then prepared *via* ATRP chain-extension using PBHME$_{10}$ as the macro-ATRP initiator and t-BA as the second monomer. The number-average molecular weights (M_n) determined by gel permeation chromatography (GPC) increased to 5600 g mol^{-1} from the original value of 5100 g mol^{-1}, and narrow molecular weight distributions (M_w/M_n) were exhibited after chain-extension (Fig. S2†). The repeating t-BA units (n) of the block copolymer were calculated based on the ^{1}H NMR spectra of the copolymer (Fig. S1†) and Formula S2,† which indicated the synthesis of the copolymer linear-PBHME$_{10}$-b-Pt-BA$_3$-Br. The linear precursor linear-PBHME$_{10}$-b-t-BA$_3$-N$_3$ was prepared from linear-PBHME$_{10}$-b-t-BA$_3$-Br *via* nucleophilic substitution reaction with NaN$_3$. Cyclic-PBHME$_{10}$-b-t-BA$_3$ was prepared *via* the copper(ı)-catalyzed azide–alkyne cycloaddition (CuAAC) of linear-PBHME$_{10}$-b-Pt-BA$_3$-N$_3$ in highly diluted DMF solutions (the detailed process is provided in the ESI†). The successful preparation of the cyclic polymer was verified by gel
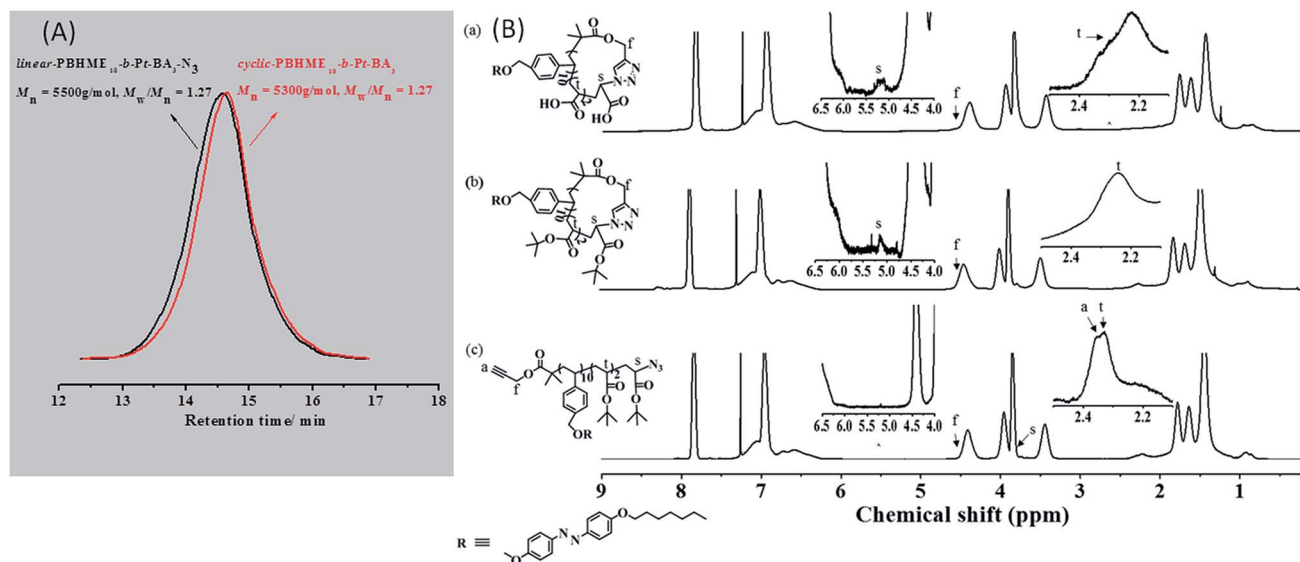
Fig. 1 (A) GPC traces of cyclic-$PBHME_{10}$-b-Pt-BA_3 and linear-$PBHME_{10}$-b-t-BA_3-N_3 using THF as the eluent. (B) ^{1}H NMR spectra of cyclic-$PBHME_{10}$-b-t-AA_3 (a), cyclic-$PBHME_{10}$-b-t-BA_3 (b), and linear-$PBHME_{10}$-b-t-BA_3-N_3 (c).

permeation chromatography (GPC), triple-detection GPC (TD-GPC), Fourier transform infrared (FTIR) and proton nuclear magnetic resonance (^{1}H NMR) spectroscopy, and matrix assisted laser desorption/ionization time of flight (MALDI-TOF) mass spectrometry. The GPC curves of cyclic-$PBHME_{10}$-b-Pt-BA_3 and its linear-precursor present a symmetric peak with a narrow molecular weight distribution (Fig. 1). The cyclic-sample shifted to a longer elution time as compared to the linear precursor; this can be attributed to the fact that the more compact cyclic architecture reduces the hydrodynamic volume. The number-average molecular weight ($M_{n,GPC}$ and $M_{n,NMR}$) of the linear- and cyclic-$PBHME_{10}$-b-Pt-BA_3 obtained by GPC measurement and calculated based on the ^{1}H NMR spectra are shown in Table 1. By monitoring the FTIR spectra, it was observed that the characteristic signals of azide at 2100 cm^{-1} and alkyne at 3300 cm^{-1} for linear-$PBHME_{10}$-b-Pt-BA_3 disappeared after CuAAC cyclization (Fig. S3(A)†). The comparison of the ^{1}H NMR spectra of the linear- and cyclic-copolymers (Fig. 1(B)) shows that the signal at around 2.3–2.4 ppm (a), which corresponds to the terminal alkynyl proton of the linear-sample, disappears in the cyclic-sample, and the characteristic

signal at around 3.7 ppm (s) adjacent to the azide group in the linear-sample shifts to 5.0–5.5 ppm after ring closure due to the formation of triazole.[59] Moreover, cyclic-$PBHME_{10}$-b-Pt-BA_3 was further confirmed by TD-GPC and MALDI-TOF mass spectrometry measurements. The number-average molecular weights ($M_{n,TD-GPC}$), absolute molecular weights ($M_{w,TD-GPC}$), intrinsic viscosity values ([η]), and hydrodynamic radius (R_h) of the linear- and cyclic-copolymers analyzed by TD-GPC are shown in Table 1 (the TD-GPC traces are displayed in Fig. S4†).[60,61] It is observed that the $M_{w,TD-GPC}$ of cyclic-$PBHME_{10}$-b-Pt-BA_3 is consistent with that of its linear precursor. Moreover, the cyclic polymer exhibits a smaller [η] value as compared to its linear counterpart; this can be ascribed to the cyclic topology. The MALDI-TOF mass spectra of cyclic- and linear-$PBHME_{10}$-b-Pt-BA_3 are shown in Fig. S5,† and the corresponding mass data are listed in Table S1.† All series of mass peaks of the linear- and cyclic-copolymers can be well assigned and are in good agreement with the theoretical peaks. These abovementioned results strongly support the successful preparation of well-defined cyclic-$PBHME_{10}$-b-Pt-BA_3.

Table 1 The number-average molecular weights (M_n), molecular weight distribution (M_w/M_n), absolute molecular weights ($M_{w,TD-GPC}$), intrinsic viscosity ([η]), and hydrodynamic radius ($R_{h,TD-GPC}$) of cyclic-$PBHME_{10}$-b-t-BA_3 and linear-$PBHME_{10}$-b-t-BA_3-N_3 determined by conventional GPC and three detection GPC (TD-GPC) as well as ^{1}H NMR spectra[a]

	GPC			TD-GPC					
	$M_{n,GPC}$ (g mol^{-1})	M_w/M_n	$M_{n,NMR}$ (g mol^{-1})	$M_{n,TD-GPC}$ (g mol^{-1})	$M_{w,TD-GPC}$ (g mol^{-1})	M_w/M_n	[η] (mL g^{-1})	$R_{h,TD-GPC}$ (nm)	dn/dc^b (mL g^{-1})
L	5500	1.27	5000	9700	11 900	1.23	5.9	2.1	0.1977
C	5300	1.27	5000	9500	11 100	1.18	5.5	2.0	0.1977

[a] L: linear-$PBHME_{10}$-b-t-BA_3-N_3, C: cyclic-$PBHME_{10}$-b-t-BA_3. [b] The dn/dc values for the linear polymer were determined by Wyatt Optilab rEX using at least three different concentrations. The dn/dc value of the cyclic polymer was assumed to be equal to that of the linear precursor.[60,61]

Selective hydrolysis of linear- and cyclic-PBHME$_m$-b-Pt-BA$_n$

The linear- and cyclic-P(BHME$_{10}$-b-t-BA$_3$) were then reacted with trifluoroacetic acid at room temperature to convert t-BA into acrylic acid (AA) via selective hydrolysis.[59] The successful selective hydrolysis was confirmed by FT-IR, ^{1}H NMR, and ^{13}C NMR (Fig. 1(B) and S3†). The ^{13}C NMR and FT-IR spectra in Fig. S3† showed that the tert-butyl ester groups entirely disappeared and transformed into carboxyl groups after the hydrolysis. Moreover, as compared to those of the ^{1}H NMR spectra of the cyclic-copolymers obtained before and after hydrolysis, the two characteristic peaks at around 4.4 ppm (f) of the methylene protons adjacent to the ester groups were exactly the same, indicating that the ester groups in the cyclic backbone were not damaged during the selective hydrolysis.

Glass transition temperature (T_g) and photoisomerization of the cyclic biblock amphiphilic copolymer in a THF solution

The glass transition temperature T_g of the linear- and cyclic-PBHME$_{10}$-b-PAA$_3$ was evaluated via differential scanning calorimetry (DSC). As shown in Table 2, the T_g of the cyclic sample was higher than that of its linear counterpart; this can be attributed to the absence of main-chain ends in the macrocycle.[42,62] Both the linear and cyclic copolymers showed only one T_g during the DSC measurement perhaps because the AA units in the block copolymers have a smaller ratio.

The photoisomerization of trans-to-cis and cis-to-trans of the linear- and cyclic-PBHME$_{10}$-b-PAA$_3$ in THF was investigated and compared under 365 nm and 435 nm light irradiation at different time intervals until the photo-stationary state was achieved (Fig. 2). The first-order kinetics curves of the photoisomerization are plotted in Fig. 3 on the basis of the Formulas S3 and S4,† and then, the rate constants (k_e and k_H) of the cyclic- and linear-PBHME$_{10}$-b-PAA$_3$ and the cyclic/linear ratio were calculated and are summarized in Table 2. The cyclic product displays larger k_e and k_H values, indicating that the cyclic sample has faster photoisomerization than its linear precursor. We speculate that the more flexible linear polymer may have a higher degree of random coil conformations as compared to the cyclic polymer without main-chain ends, which probably leads a more transition resistance for its trans-to-cis isomerization.[14,48]
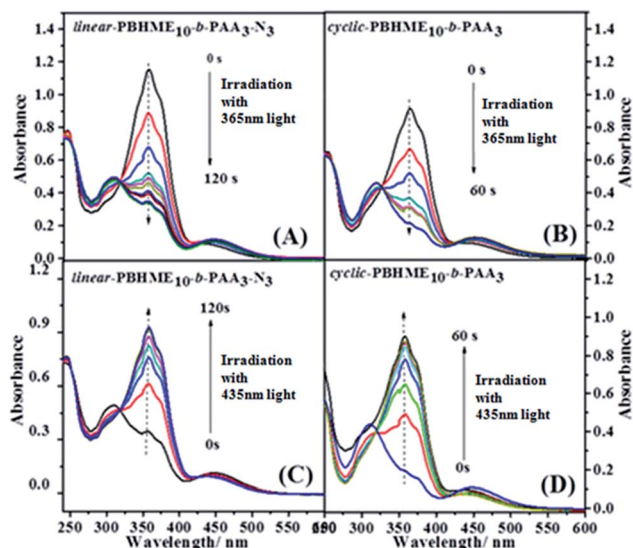

Fig. 2 UV-vis absorption changes of linear- and cyclic-PBHME$_{10}$-b-PAA$_3$ in THF at different time intervals as a function of 365 nm (1 mW cm^{-2}) (A and B) and 435 nm (60 mW cm^{-2}) (C and D) light irradiation at room temperature, respectively. The concentration of the solution is 2.0×10^{-5} g mL^{-1}.
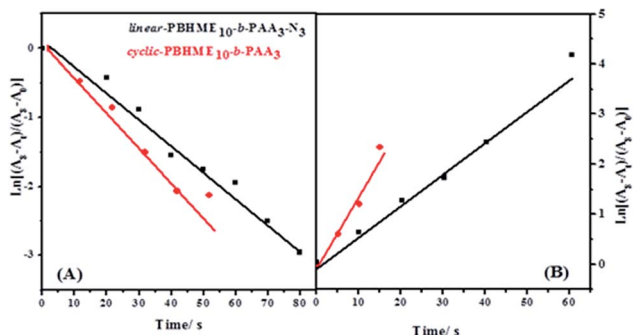

Fig. 3 First-order kinetic curves for the trans-to-cis photo-isomerization of linear- and cyclic-PBHME$_{10}$-b-PAA$_3$ during irradiation with 365 nm UV light (1 mW cm^{-2}) (A) and first-order kinetics curves for cis-to-trans recovery during irradiation with 435 nm light (60 mW cm^{-2}) (B). The concentration of the polymers in THF is 2.0×10^{-5} g mL^{-1}.

Self-assembly behaviors and photo-responsive performance of the aggregates from linear- and cyclic-PBHME$_m$-b-PAA$_n$

The self-assembly behavior of cyclic-PBHME$_{10}$-b-PAA$_3$ was investigated using a mixture solution of water/THF. The self-assembly of the linear precursor was conducted under the same conditions as its cyclic counterpart to identify the influence of the cyclic structure on its properties. A representative self-assembly solution was directly prepared by slowly adding water to a solution of the polymer in THF with an initial concentration of 0.20 mg mL^{-1} until the mixture solution reached the ratio of 3/10 (v/v) of water/THF. The morphology and sizes of the self-assembled micellar aggregates were verified via transmission electron microscopy (TEM) and dynamic light scattering (DLS). Both the cyclic and linear amphiphilic

Table 2 Glass transition temperatures (T_g) of linear- and cyclic-PBHME$_{10}$-b-PAA$_3$ determined by differential scanning calorimetry (DSC) and kinetic parameters for the trans-to-cis and cis-to-trans isomerization of linear- and cyclic-PBHME$_{10}$-b-PAA$_3$ in THF solution[e]

Sample	T_g, °C	ΔT_g, °C	$k_e{}^a \times 10^{-3}$ s^{-1}	$k_e/ k'_e{}^b$	$k_H{}^c \times 10^{-4}$ s^{-1}	$k_H/ k'_H{}^d$
L	44	11	2.25	2.43	0.62	1.98
C	55		5.46		1.23	

[a] Rate constant of trans-to-cis photoisomerization. [b] Rate constant ratio of trans-to-cis isomerization of the cyclic-polymer relative to the linear-polymer. [c] Rate constant of trans-to-cis recovery. [d] Rate constant ratio of cis-to-trans recovery of the cyclic-polymer relative to the linear-polymer. [e] L: linear-PBHME$_{10}$-b-PAA$_3$-N$_3$ and C: cyclic-PBHME$_{10}$-b-PAA$_3$.
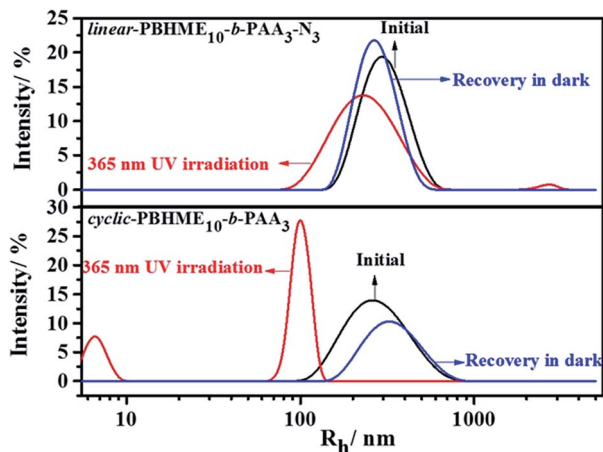
Fig. 4 Hydrodynamic radius (R_h) distribution of the aggregates formed by linear-PBHME$_{10}$-b-PAA$_3$-N$_3$ and cyclic-PBHME$_{10}$-b-PAA$_3$ upon 365 nm light irradiation (50 μW cm^{-2}) and stored in the dark for an appropriate period of time.

polymers formed spherical aggregates *via* self-assembly in the water/THF mixture solution (Fig. 4 and 5). The aggregate sizes of the cyclic and linear copolymers were both around 150 ± 30 nm, as observed from the TEM image, and about 550 nm, as observed from the hydrodynamic diameters measured by DLS. The sizes obtained *via* TEM are smaller than those obtained from DLS owing to sample shrinkage during the sample preparation process for TEM measurements. Subsequently, the photo-responsive behaviors of the self-assembled aggregates were investigated by the *trans*-to-*cis* photoisomerization of azobenzene under UV light irradiation (365 nm, 1 mW cm^{-2}) and then thermally-driven *cis*-to-*trans* return by placing the
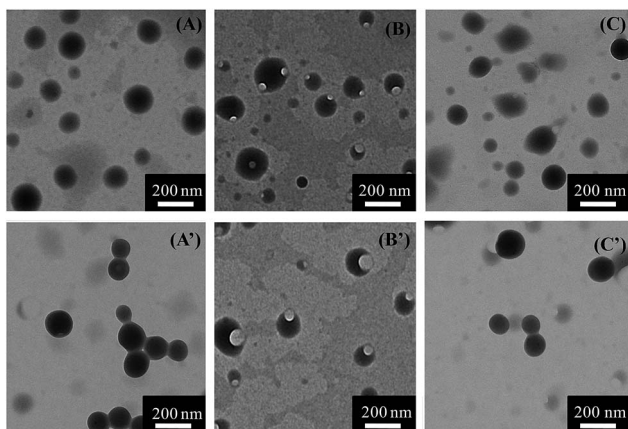
irradiated sample in the dark at room temperature until the photo-stationary states were reached. Moreover, the UV-vis absorption spectra of the aggregate solutions under the above-mentioned condition of photoisomerization were obtained. As shown in Fig. 6, the absorbance at around 450 nm corresponding to the *cis* isomers increased gradually together with a decrease in the absorbance at around 358 nm, which corresponded to the *trans* isomers upon UV light irradiation. Then, *cis*-to-*trans* isomerization reversal occurred when the irradiated sample was placed in the dark. It was noted that a portion of the spherical aggregates of both the linear- and cyclic-polymers became smaller after exposing the aggregate solutions to 365 nm light, and then, most of the aggregates re-formed after thermally-driven back-isomerization in the dark for a period of time (Fig. 5). The photo-responsive behavior of the aggregates was further confirmed by DLS measurement, which showed that the aggregate sizes reduced to around 450 nm for the linear structure and 220 nm for the cyclic structure from the initial size of 550 nm upon UV light irradiation, and then, both sizes recovered and became slightly larger (about 660 nm) after thermal *cis*-to-*trans* relaxation. In addition, gaps appeared outside of the spherical aggregates after UV light irradiation, and especially distinct larger gaps similar to holes were observed for the cyclic-sample as compared to those for the linear sample. The reversible changing of disruption and re-formation of micellar aggregates can be attributed to the unique *trans*-to-*cis* photoisomerization of azobenzene. The curved *cis*-configuration of azobenzene has a larger dipole moment and a shorter length between the 4 and 4′ positions of two benzene rings as compared to the clavated *trans*-configuration. The variation in the configuration and polarity between the *trans* and *cis* isomers of azobenzene mesogens can transform the hydrophilic/hydrophobic balance of amphiphilic copolymers in selective solvents during the *trans*-to-*cis* isomerization process. Upon UV light irradiation, the hydrophobic PBHME block in the micellar aggregates formed a more
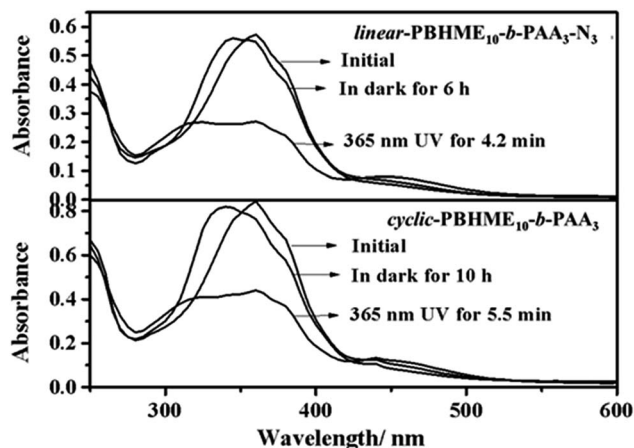

Fig. 5 TEM images of the spherical aggregates of linear and cyclic-PBHME$_{10}$-b-PAA$_3$ formed in H$_2$O/THF solvent (initial concentration: 0.20 mg mL^{-1} in THF solvent; H$_2$O/THF (v/v) = 3/10). (A) Initial aggregates formed by linear-PBHME$_{10}$-b-PAA$_3$; (A′) initial aggregates formed by cyclic-PBHME$_{10}$-b-PAA$_3$; (B) aggregates formed by linear-PBHME$_{10}$-b-PAA$_3$ after UV irradiation for 4.2 min; (B′) aggregates formed by cyclic-PBHME$_{10}$-b-PAA$_3$ after UV irradiation for 5.5 min; (C) aggregates of the irradiated linear-PBHME$_{10}$-b-PAA$_3$ after storage in the dark for 6 h and (C′) aggregates of the irradiated cyclic-PBHME$_{10}$-b-PAA$_3$ after storage in the dark for 10 h.

Fig. 6 UV-vis absorption changes for linear-PBHME$_{10}$-b-PAA$_3$-N$_3$ and cyclic-PBHME$_{10}$-b-PAA$_3$ in THF/water solution under 365 nm UV light irradiation (50 μW cm^{-2}) and after the irradiated sample was placed in the dark at room temperature. The concentration of the solutions was 2.0 × 10^{-5} g mL^{-1}.

compact region because of its configuration change *via trans*-to-*cis* photoisomerization.[26] As a result, the THF solvent, which was wrapped in the aggregates, diffused into the solution, resulting in gaps. The cyclic structure exhibits more sensitive photo-responsive properties such as larger changes in the size and morphology of the aggregate micelles as compared to the linear structure upon 365 nm light irradiation. We speculate that the cyclic amphiphile may self-assemble into relatively loose aggregates due to the rigidity of its main chain, which is imposed by the cyclic conformation, as compared to the linear amphiphile.[51,53]

Conclusions

In summary, well-defined cyclic block copolymers bearing hydrophobic azobenzene and hydrophilic carboxyl moieties in their side-chains, cyclic-PBHME$_m$-*b*-PAA$_n$, were successfully prepared *via* sequential ATRP and intramolecular CuAAC cyclization reaction followed by the selective hydrolysis of *tert*-butyl ester. The investigations on the amphiphilic block macrocycles indicate that the cyclic amphiphilic biblock copolymers display faster photoisomerization of *trans*-to-*cis* and *cis*-to-*trans* in THF than their linear precursors. In addition, the self-assembled micellar aggregates of the cyclic architecture in the mixture solution of water/THF exhibit larger changes in size and morphology upon 365 nm light irradiation as compared to those of their linear counterparts. These interesting differences between the cyclic- and linear copolymers could be attributed to the topological cyclic architecture, which indicated that the cyclic architecture greatly affected the photoisomerization of azobenzene and polymeric packing behaviors in micellar aggregates. This study provides new insight into the structure–property relationship and gives guidance to future designs for the development of responsive-related functional materials. Further studies aimed at functional polymers based on azobenzene are being conducted by our research group.

Acknowledgements

Notes and references

1 Y. Mai and A. Eisenberg, *Chem. Soc. Rev.*, 2012, **41**, 5969–5985.

2 K. Yu and A. Eisenberg, *Macromolecules*, 1998, **31**, 3509–3518.

3 D. Chen and M. Jiang, *Acc. Chem. Res.*, 2005, **38**, 494–502.

4 Z. Ge and S. Liu, *Chem. Soc. Rev.*, 2013, **42**, 7289–7325.

5 C. Allen, Y. Yu, D. Maysinger and A. Eisenberg, *Bioconjugate Chem.*, 1998, **9**, 564–572.

6 Z. Zhang, R. Ma and L. Shi, *Acc. Chem. Res.*, 2014, **47**, 1426–1437.

7 C. Allen, D. Maysinger and A. Eisenberg, *Colloids Surf., B*, 1999, **16**, 3–27.

8 D. Han, X. Tong and Y. Zhao, *Macromolecules*, 2011, **44**, 437–439.

9 E. Fleige, M. Quadir and R. Haag, *Adv. Drug Delivery Rev.*, 2012, **64**, 866–884.

10 J. Hu and S. Liu, *Macromolecules*, 2010, **43**, 8315–8330.

11 J. Jiang, X. Tong and Y. Zhao, *J. Am. Chem. Soc.*, 2005, **127**, 8290–8291.

12 S. Uchiyama and Y. Makino, *Chem. Commun.*, 2009, **19**, 2646–2648.

13 Y. Zhao and T. Ikeda, *Smart Light responsive Materials Azobenzene-Containing Polymers and Liquid Crystals*, John Wiley & Sons, Inc., Hoboken, New Jersey, 2009.

14 A. Beharry and G. Woolley, *Chem. Rev.*, 1989, **89**, 1915–1925.

15 O. Sadovski, A. Beharry, F. Zhang and G. A. Woolley, *Angew. Chem., Int. Ed.*, 2009, **48**, 1484–1486.

16 A. Beharry and G. Woolley, *Chem. Soc. Rev.*, 2011, **40**, 4422–4437.

17 H. Rau, *Angew. Chem., Int. Ed.*, 1973, **12**, 224–235.

18 J. Lu, F. Zhou, L. Li, Z. Zhang, F. Meng, N. Zhou and X. Zhu, *RSC Adv.*, 2016, **6**, 58755–58763.

19 S. Luo, Y. Liu, F. Wang, Q. Fei, B. Shi, J. An, C. Zhao and C. H. Tung, *Analyst*, 2016, **141**, 2879–2882.

20 J. Rao, C. Hottinger and A. Khan, *J. Am. Chem. Soc.*, 2014, **136**, 5872–5875.

21 A. Wong, A. Prinzen and E. Gillies, *Polym. Chem.*, 2016, **7**, 1871–1881.

22 Y. Zhao, *Macromolecules*, 2012, **45**, 3647–3657.

23 R. Dong, B. Zhu, Y. Zhou, D. Yan and X. Zhu, *Polym. Chem.*, 2013, **4**, 912–915.

24 K. Han, W. Su, M. Zhong, Q. Yan, Y. Luo, Q. Zhang and Y. Li, *Macromol. Rapid Commun.*, 2008, **29**, 1866–1870.

25 X. Tong, G. Wang, A. Soldera and Y. Zhao, *J. Phys. Chem. B*, 2005, **109**, 20281–20287.

26 D. Wang and X. Wang, *Prog. Polym. Sci.*, 2013, **38**, 271–301.

27 E. Blasco, B. V. K. J. Schmidt, C. Barner-Kowollik, M. Pinol and L. Oriol, *Macromolecules*, 2014, **47**, 3693–3700.

28 W. Sun, X. He, C. Gao, X. Liao, M. Xie, S. Lin and D. Yan, *Polym. Chem.*, 2013, **4**, 1939–1949.

29 J. A. Lv, Y. Liu, J. Wei, E. Chen, L. Qin and Y. Yu, *Nature*, 2016, **537**, 179–184.

30 R. Walker, H. Audorff, L. Kador and H. Schmidt, *Adv. Funct. Mater.*, 2009, **19**, 2630–2638.

31 J. Lu, A. Xia, N. Zhou, W. Zhang, Z. Zhang, X. Pan, Y. Yang, Y. Wang and X. Zhu, *Chem.–Eur. J.*, 2015, **21**, 2324–2329.

32 S. Iamsaard, S. J. Asshoff, B. Matt, T. Kudernac, J. Cornelissen, S. P. Fletcher and N. Katsonis, *Nat. Chem.*, 2014, **6**, 229–235.

33 J. Lu, G. Jiang, Z. Zhang, W. Zhang, Y. Yang, Y. Wang, N. Zhou and X. Zhu, *Polym. Chem.*, 2015, **6**, 8144–8149.

34 P. Weis, D. Wang and S. Wu, *Macromolecules*, 2016, **49**, 6368–6373.

35 Y. Zhao and J. He, *Soft Matter*, 2009, **5**, 2686–2693.

36 K. Zhang, M. A. Lackey, J. Cui and G. N. Tew, *J. Am. Chem. Soc.*, 2011, **133**, 4140–4148.

37 S. Honda, T. Yamamoto and Y. Tezuka, *Nat. Commun.*, 2013, **4**, 1–9.

38 S. H. Lahasky, X. Hu and D. Zhang, *ACS Macro Lett.*, 2012, **1**, 580–584.

39 J. Poelma, K. Ono, D. Miyajima, T. Aida, K. Satoh and C. J. Hawker, *ACS Nano*, 2012, **6**, 10845–10854.

40 X. Zhu, N. Zhou, Z. Zhang, B. Sun, Y. Yang, J. Zhu and X. Zhu, *Angew. Chem., Int. Ed.*, 2011, **50**, 6615–6618.

41 X. Wan, T. Liu and S. Liu, *Biomacromolecules*, 2011, **12**, 1146–1154.

42 M. D. Hossain, D. Lu, Z. Jia and M. J. Monteiro, *ACS Macro Lett.*, 2014, **3**, 1254–1257.

43 M. A. Cortez, W. T. Godbey, Y. Fang, M. E. Payne, B. J. Cafferty, K. A. Kosakowska and S. M. Grayson, *J. Am. Chem. Soc.*, 2015, **137**, 6541–6549.

44 C. W. Bielawski, D. Benitez and R. H. Grubbs, *Science*, 2002, **297**, 2041–2044.

45 H. Zhang, W. Wu, X. Zhao and Y. Zhao, *Macromolecules*, 2017, **50**, 3411–3423.

46 D. Han, X. Tong, Y. Zhao, T. Galstian and Y. Zhao, *Macromolecules*, 2010, **43**, 3664–3671.

47 H. Zhang, N. Zhou, X. Zhu, X. Chen, Z. Zhang, W. Zhang, J. Zhu, Z. Hu and X. Zhu, *Macromol. Rapid Commun.*, 2012, **33**, 1845–1851.

48 Y. Sun, Z. Wang, Y. Li, Z. Zhang, W. Zhang, X. Pan, N. Zhou and X. Zhu, *Macromol. Rapid Commun.*, 2015, **36**, 1341–1347.

49 K. Heo, Y. Y. Kim, Y. Kitazawa, M. Kim, K. S. Jin, T. Yamamoto and M. Ree, *ACS Macro Lett.*, 2014, **3**, 233–239.

50 R. J. Williams, A. Pitto-Barry, N. Kirby, A. P. Dove and R. K. O'Reilly, *Macromolecules*, 2016, **49**, 2802–2813.

51 X. Fan, B. Huang, G. Wang and J. Huang, *Macromolecules*, 2012, **45**, 3779–3786.

52 S. Honda, T. Yamamoto and Y. Tezuka, *J. Am. Chem. Soc.*, 2010, **132**, 10251–10253.

53 D. E. Lonsdale and M. J. Monteiro, *J. Polym. Sci., Part A: Polym. Chem.*, 2011, **49**, 4603–4612.

54 Y. Dong, Y. Tong, B. Dong, F. Du and Z. Li, *Macromolecules*, 2009, **42**, 2940–2948.

55 M. Schappacher and A. Deffieux, *Science*, 2008, **319**, 1512–1515.

56 Y. Li, H. Su, X. Feng, K. Yue, Z. Wang, Z. Lin, X. Zhu, Q. Fu, Z. Zhang, S. Z. D. Cheng and W. Zhang, *Polym. Chem.*, 2015, **6**, 827–837.

57 B. Laurent and S. Grayson, *J. Am. Chem. Soc.*, 2006, **128**, 4238–4239.

58 G. Huang, J. Zhu, Z. Zhang, W. Zhang, N. Zhou and X. Zhu, *J. Macromol. Sci., Part A: Pure Appl. Chem.*, 2013, **50**, 193–199.

59 Y. Cai, J. Lu, F. Zhou, X. Zhou, N. Zhou, Z. Zhang and X. Zhu, *Macromol. Rapid Commun.*, 2014, **35**, 901–907.

60 H. Durmaz, A. Dag, G. Hizal and U. Tunca, *J. Polym. Sci., Part A: Polym. Chem.*, 2011, **49**, 1195–1200.

61 H. Durmaz, A. Dag, G. Hizal and U. Tunca, *J. Polym. Sci., Part A: Polym. Chem.*, 2010, **48**, 5083–5091.

62 G. Nossarev and T. Hogen-Esch, *Macromolecules*, 2002, **35**, 1604–1610.